

# Sr<sub>2</sub>RuO<sub>4</sub>, like doped cuprates and barium bismuthate, is a negative charge-transfer gap even parity superconductor with $\frac{3}{4}$ -filled oxygen band

Sumit Mazumdar<sup>1,2,3</sup>

<sup>1</sup>*Department of Physics, University of Arizona Tucson, AZ 85721*

<sup>2</sup>*Department of Chemistry and Biochemistry, University of Arizona, Tucson, AZ 85721*

<sup>3</sup>*College of Optical Sciences, University of Arizona, Tucson, AZ 85721*

(Dated: February 21, 2020)

The valence transition model, recently proposed for the superconducting cuprates [Phys. Rev. B **98**, 205153] is extended to Sr<sub>2</sub>RuO<sub>4</sub>. It is argued that even as Ru-ions occur as low-spin Ru<sup>4+</sup> in the Mott-Hubbard semiconductor CaRu<sub>2</sub>O<sub>4</sub>, in metallic Sr<sub>2</sub>RuO<sub>4</sub> they occur as high-spin Ru<sup>3+</sup>. The insulator-to-metal transition is distinct from that expected from the simple “melting” of the Mott-Hubbard semiconductors. The half-filled Ru<sup>3+</sup> ions in Sr<sub>2</sub>RuO<sub>4</sub> with very high ionization energy contribute to magnetism but not transport. The charge carriers are entirely on the layer oxygen ions, which have an average charge  $-1.5$ . Spin-singlet superconductivity in Sr<sub>2</sub>RuO<sub>4</sub> evolves from the correlated lattice-frustrated  $\frac{3}{4}$ -filled band of layer oxygen ions alone, in agreement with quantum many-body calculations that have demonstrated enhancement by electron-electron interactions of superconducting pair-pair correlations uniquely at or very close to this filling [Phys. Rev. B **93**, 165110 and **93**, 205111]. The model simultaneously predicts  $d$ -wave superconductivity in Sr<sub>2</sub>RuO<sub>4</sub> and explains the apparent breaking of time reversal symmetry that is unrelated to superconductivity. The model also explains the unprecedented giant diamagnetism in the semimetallic state reached by passing small current through insulating Ca<sub>2</sub>RuO<sub>4</sub>. Several model-specific experimental predictions are made, including that spin susceptibility due to Ru-ions will remain unchanged as Sr<sub>2</sub>RuO<sub>4</sub> is taken through superconducting T<sub>c</sub>.

PACS numbers:

## I. INTRODUCTION.

Sr<sub>2</sub>RuO<sub>4</sub> has long been thought of as a chiral spin-triplet superconductor, with orbital parity  $p_x \pm ip_y$ <sup>1</sup>. This viewpoint has recently been challenged by multiple experiments<sup>2-8</sup> that are beginning to lead to a thorough re-examination of earlier experiments or their interpretations and theories. A few investigators have even suggested that the superconducting pairing might have even parity, likely  $d$ -wave<sup>6</sup>. In the present theoretical work, which is an extension of a valence transition model<sup>9</sup> recently postulated for superconducting cuprates and doped barium bismuthate, (Ba,K)BiO<sub>3</sub>, I posit that the peculiarities observed in Sr<sub>2</sub>RuO<sub>4</sub> should not be considered in isolation, but that the unconventional behaviors of all these superconducting perovskite oxides, along with the pseudogap-like features<sup>10-12</sup> observed in electron-doped Sr<sub>2</sub>IrO<sub>4</sub>, can be understood within a common theoretical model. The key theoretical features of this theory are valence transition and negative charge-transfer gap, which in all cases are driven by a unique property common to the materials of interest: the essential cation in each material has a strong tendency to have true ionicity lower than the formal ionicity by a full integer unit. This is a strong correlations effect that is missed in band or first principles calculations, which find mixed valence as opposed to distinct phases with integer valence. The insulator-to-metal transition (IMT) in these systems is different from that arising from simple “doping” or “self-doping” of a semiconductor, as has been assumed until now. Within the proposed model

the insulating phase has the usual  $M^{n+}(O^{2-})_2$  intralayer unit cell composition, but the true (as opposed to formal) ionic composition in the pseudogap and metallic states is  $M^{(n-1)+}(O^{1.5-})_2$ . As a consequence of the valence transition, in all cases the pseudogap state (wherever applicable) and the “normal” state from which superconductivity (SC) emerges consist of a strongly correlated oxygen (O)-band in which nearly half the oxygens (as opposed to a few) have ionicities  $O^{1-}$ . The cations in their true ionicities are either closed-shell or exactly half-filled and play no role in SC.

The negative charge-transfer gap model is arrived at from heuristic arguments as opposed to direct computations, as the sheer number of many-body interactions and parameters that would enter such computations are enormously large (the relative magnitudes of the different parameters that would enter a complete theoretical model are known however). The validity of the model can therefore be tested only by comparing theoretically arrived at conclusions against existing experiments as well as new experiments that are performed to test predictions of the theory. It then becomes necessary to list the full set of experiments that any theory that claims to be comprehensive should be able to explain at least qualitatively. This is the approach that was taken in the earlier work on the cuprates<sup>9</sup> and is taken here for Sr<sub>2</sub>RuO<sub>4</sub>. In the next section I list what I believe are the most challenging observations, including apparent contradictions, in (i) Sr<sub>2</sub>RuO<sub>4</sub>, (ii) the isoelectronic Mott-Hubbard semiconductor Ca<sub>2</sub>RuO<sub>4</sub> and the temperature, pressure and most importantly, current-driven IMT in this, and the

(iii)  $x$ -dependent behavior of  $\text{Ca}_{2-x}\text{Sr}_x\text{RuO}_4$ . Following this in section III I briefly present the theory of what I term as type I negative charge-transfer gap, as observed in doped cuprates,  $\text{BaBiO}_3$  and  $(\text{Ba,K})\text{BiO}_3$ , and doped  $\text{Sr}_2\text{IrO}_4$  in octahedral environment. Although much of this has already been presented in the earlier work<sup>9</sup>, it is necessary to repeat this briefly here to point out the unique common feature shared by  $\text{Cu}^{1+}$ ,  $\text{Bi}^{3+}$ ,  $\text{Ir}^{3+}$  in octahedral environment, and  $\text{Ru}^{3+}$ . It is this shared feature that is the driver of an unusual IMT in these perovskite oxides. Section IV discusses the physical mechanism behind the valence transition that drives what I term as the type II negative charge-transfer gap in  $\text{Sr}_2\text{RuO}_4$ . Section V shows how all the experiments listed in section II, in particular spin-singlet even parity SC and apparent breaking of time reversal symmetry can be simultaneously understood within the theoretical model. Finally in section VI I make experimental testable predictions on  $\text{Sr}_2\text{RuO}_4$  that are completely specific to the negative charge-transfer gap model. Section VII presents the conclusions, focusing in particular to the unique features of the correlated  $\frac{3}{4}$ -filled band.

## II. THEORETICAL CHALLENGES

### A. Experimental puzzles, $\text{Sr}_2\text{RuO}_4$ .

(i)  $T_c$  enhancement under uniaxial pressure. The superconducting critical temperature  $T_c$  in  $\text{Sr}_2\text{RuO}_4$  crystals is strongly enhanced upon the application of uniaxial pressure along the [100] direction<sup>3-5</sup>, even as hydrostatic pressure suppresses  $T_c$ . Starting from the ambient pressure value of 1.5 K,  $T_c$  reaches a peak value of 3.4 K at uniaxial compression of 0.6%, following which  $T_c$  decreases again. Based on band structure calculations it has been suggested the peak in  $T_c$  corresponds to the compression at which the Fermi level crosses the van Hove singularity<sup>5</sup>. Theoretically predicted splitting of the transition temperatures due to separate  $p_x$  and  $p_y$  components were not observed. The superconducting transition at the maximum  $T_c$  is very sharp, allowing precise determinations of the upper critical fields for magnetic fields both along the intra-plane [100] direction ( $H_{c2||a}$ ) as well as perpendicular to the plane ( $H_{c2||c}$ ). While  $H_{c2||c}$  is enhanced by more than a factor of 20 relative to unstrained  $\text{Sr}_2\text{RuO}_4$ , in-plane  $H_{c2||a}$  is enhanced by only a factor of 3. Importantly, for the spins lying in the (2D) plane, neither orbital limiting nor Pauli limiting should apply to  $H||a$ , and  $H_{c2||a}/H_{c2||c}$  should be infinite within the existing spin and orbital characterization of the superconducting state. *The observed ratio of only about 3 in the strained material casts severe doubts about the chiral  $p$ -wave symmetry.*

(ii)  $^{17}\text{O}$  NMR. The earlier experiment that had given the most convincing evidence for triplet SC was based on the measurement of the O-ion Knight-shift as a function of temperature<sup>13</sup>. No change in spin susceptibility

was detected as the sample was taken through the critical temperature  $T_c$ . Luo *et al.*<sup>7</sup> and Pustogow *et al.*<sup>8</sup> have repeated the  $^{17}\text{O}$  NMR measurements in uniaxially compressed  $\text{Sr}_2\text{RuO}_4$  for different strain levels<sup>3-5</sup>, inclusive of the complete range of  $T_c = 1.5 - 3.4$  K. Reduction in the Knight shift, and therefore drop in the spin susceptibility have been found for all strains, including for the unstrained sample<sup>8</sup>. Most importantly, *the NMR study finds no evidence for a transition between different symmetries.* The experiment conclusively precludes  $p_x \pm ip_y$  triplet pairing, and leaves open the possibilities of helical triplet pairings, spin-singlet  $d_{xy}$  or  $d_{x^2-y^2}$  pairings and chiral  $d$ -wave pairing.

(iii) *Breaking of time reversal symmetry.* Muon-spin rotation<sup>14</sup> and magneto-optic polar Kerr rotation<sup>15</sup> measurements had suggested that time-reversal symmetry is broken upon entering the superconducting state. This conclusion has been contradicted by recent observation that the Josephson critical current is invariant under the inversion of current and magnetic fields<sup>16</sup>. It is relevant in this context that the polar Kerr effect is also seen in hole-doped cuprates inside the pseudogap, and while originally this was also ascribed to time reversal symmetry breaking, it has been later ascribed to two-dimensional (2D) chirality<sup>17</sup>.

(iv) *Magnetocaloric and thermal conductivity measurements.* Magnetocaloric measurements have found that the superconductor-to-metal transition in the unstrained material at  $T \simeq 0.5T_c$  is first order, indicating that the pair-breaking is Pauli-limited, *i.e.*, pairing is spin-singlet<sup>18</sup>. Among the symmetries not precluded by the  $^{17}\text{O}$  NMR experiment<sup>8</sup> the helical triplet orders and the chiral  $d$ -wave order have horizontal nodes while the  $d_{xy}$  and  $d_{x^2-y^2}$  orders have vertical nodes. Recent thermal conductivity measurements have found evidence for vertical line nodes consistent with  $d$ -wave pairing<sup>6</sup>.

### B. Experimental puzzles, $\text{Ca}_2\text{RuO}_4$ and $\text{Ca}_{2-x}\text{Ru}_x\text{O}_4$ .

Replacement of Sr with Ca generates the isoelectronic  $\text{Ca}_2\text{RuO}_4$  as well as the “doped” compounds  $\text{Ca}_{2-x}\text{Sr}_x\text{RuO}_4$ ,  $0 \leq x \leq 2$ .  $\text{Ca}_2\text{RuO}_4$  is an antiferromagnetic semiconductor with energy gap between 0.2 - 0.4 eV at low temperatures<sup>19-22</sup>. Ru-ions in this compound have ionicity +4 and are in the low-spin state, with  $4d$  orbital occupancy  $t_{2g}^4$ . Néel temperature of 113 K and paramagnetic semiconductor to paramagnetic metal transition at  $\sim 360$  K show that the system is a Mott-Hubbard semiconductor. The mechanism of the Mott-Hubbard IMT remains controversial but one popular mechanism involves increased  $d_{xy}$ -occupancy to upto 2 electrons due to Jahn-Teller distortion, with Hund’s rule coupling leading to 1 electron each in the  $d_{xz}$  and  $d_{yz}$  orbitals<sup>21,23,24</sup>. The half-filled nature of the  $d_{xz}$  and  $d_{yz}$  bands then lead to Mott-Hubbard semiconducting behavior. The transition is accompanied with

structural distortions involving tilts and rotations of the  $\text{RuO}_6$  octahedra, with the layer (apical) Ru-O bonds becoming shorter (longer) in the metallic phase (*i.e.* the metallic phase is more 2D than the semiconducting antiferromagnet)<sup>20</sup>. Similar structural changes are also seen in pressure-induced insulator-to-metal transition, where, however, the metallic state has been found to be proximate to ferromagnetism<sup>25</sup>. “Doping”-induced IMT occurs in  $\text{Ca}_{2-x}\text{Sr}_x\text{RuO}_4$  for  $x > 0.2$ . Importantly, the high temperature metallic phase in  $\text{Ca}_2\text{RuO}_4$ , the paramagnetic metallic phase  $0.5 \leq x \leq 1.5$  and the  $x = 2$  phase pure  $\text{Sr}_2\text{CuO}_4$  are all structurally different.

An unprecedented electric field-induced IMT, with a lower threshold field of 40 V/cm tiny compared to the known semiconducting gap of 0.2 - 0.4 eV has been found in  $\text{Ca}_2\text{RuO}_4$ <sup>26,27</sup>. The small magnitude of the threshold field, taken together with the even more surprising strong current-induced diamagnetism<sup>28</sup> in the semimetallic state reached with a current density as low as 1 A/cm<sup>2</sup> suggest that the current-induced metallic state is different from the one reached by the usual “melting” of a Mott-Hubbard semiconductor. This is further confirmed by diffraction studies that have established that *the crystal structure of the current-induced semimetallic state is different from the state reached by applications of temperature, pressure or strain*<sup>29</sup>.

In summary, a theory of SC in  $\text{Sr}_2\text{RuO}_4$  must reconcile experiments that indicate spin-singlet *d*-wave SC on the one hand and others that find broken time-reversal symmetry. Additionally the theory should explain the novel current-induced IMT and diamagnetism in  $\text{Ca}_2\text{RuO}_4$ .

### III. CUPRATES, BISMUTHATE AND IRIDATES: TYPE I NEGATIVE CHARGE-TRANSFER GAP.

The central postulate of the present work is that the peculiarities observed in  $\text{Sr}_2\text{RuO}_4$  should not be considered in isolation, as equally perplexing mysteries persist with the other perovskite superconductors cuprates and (Ba,K)BiO<sub>3</sub>, and in the pseudogap-like state<sup>10-12</sup> in electron-doped  $\text{Sr}_2\text{IrO}_4$ . I argue in this subsection that the failure to arrive at a comprehensive theory in every case stems from focusing on *cation-centric Hamiltonians* (for e.g., the single-band Hubbard model for cuprates). In the following I first list the experiments in the cuprates, (Ba,K)BiO<sub>3</sub> and  $\text{Sr}_2\text{IrO}_4$  that most strongly argue against cation-centric Hamiltonians. Following this a brief presentation of the theory behind negative charge-transfer gap<sup>9</sup> in these systems is presented.

#### A. The need to go beyond cation-centric models

(i) The simultaneous breaking of rotational and translational symmetries in the hole-doped T-phase cuprates, accompanied by intra-unit cell O-ion inequivalency<sup>30-33</sup>

illustrate most strongly the need to incorporate the O-ions in any starting theoretical description of the cuprates. With the T' compounds, the most peculiar features are (i) the very robust antiferromagnetism in the “usual” electron-doped materials<sup>34</sup>, (ii) the appearance of SC at zero doping nevertheless in specially prepared thin film samples, with  $T_c$  higher than the maximum  $T_c$  in the “usual” materials<sup>35</sup>, and (iii) charge-order with *nearly the same periodicity as the hole-doped cuprates*<sup>36,37</sup>. Taken together, these observations present the following conundrum. On the one hand, inequivalent O-ions in the hole-doped compounds in the charge-ordered state from which the superconducting states emerge require that the O-ions are included in any attempt to construct a comprehensive theoretical model. On the other, the apparent symmetry between the hole- and electron-doped compounds (in so far as SC is concerned) *requires* explanation within a single-band model, since electron-hole symmetry is absent within multiband models.

(ii) Negative charge-transfer gap in  $\text{BaBiO}_3$  is already recognized. The semiconducting gap in undoped  $\text{BaBiO}_3$  within traditional cation-centric models<sup>38</sup> had been ascribed to a charge-density wave (CDW) consisting of alternate  $\text{Bi}^{3+}$  and  $\text{Bi}^{5+}$ -ions. SC in  $\text{Ba}_{1-x}\text{K}_x\text{BiO}_3$  within these models emerges from doping the parent Bi-based CDW. Recent theoretical and experimental demonstrations<sup>39,40</sup> of the occurrence of Bi-ions exclusively as  $\text{Bi}^{3+}$  show convincingly that the existing theories of SC are simplistic. There is also no explanation of the limitation of SC<sup>39,41</sup> to K-concentration  $0.37 \leq x \leq 0.5$  in  $\text{Ba}_{1-x}\text{K}_x\text{BiO}_3$ , an issue to which we return later.

(iii)  $\text{Sr}_2\text{IrO}_4$  has attracted strong attention in recent years as an effective square lattice Mott-Hubbard insulator. The active layer consists of  $\text{IrO}_2$  unit cells with nominally tetravalent  $\text{Ir}^{4+}$ . The *d*-electron occupancy is  $t_{2g}^5$  as a consequence of large crystal field stabilization energy (CFSE). The  $t_{2g}$  orbitals are split by spin-orbit coupling into lower twofold degenerate total angular momentum  $J_{eff} = \frac{3}{2}$  levels and an upper nondegenerate narrow  $J_{eff} = \frac{1}{2}$  level<sup>42</sup>. Occupancy of the latter by a single unpaired electron explains the Mott-Hubbard like behavior of undoped  $\text{Sr}_2\text{IrO}_4$ . Remarkable similarities<sup>10-12,43</sup> are found between hole-doped cuprates in the pseudogap phase and and electron-doped  $\text{Sr}_2\text{IrO}_4$ . Following the vanishing of the Mott-Hubbard gap at  $\sim 5\%$  doping there appears a *d*-wave like gap in the nodal region, with strong deviation in the antinodal region, where the gap is much larger<sup>12</sup>, exactly as in the cuprates<sup>44</sup>. Theoretical attempts to explain these observations borrow heavily from the single-band Hubbard model description for cuprates, which, we have pointed out, is at best incomplete.

(iv) Although this subsection has focused on experiments, it is useful to point out a crucial recent theoretical development. Convincing proof of the absence of SC in the weakly doped 2D Hubbard Hamiltonian with

nearest neighbor-only hoppings has been found from a comprehensive study that used two different complementary many-body techniques<sup>45</sup>. While reference 45 leaves open the possibility that SC might still appear within a more complex Hubbard model with next-nearest neighbor hopping, calculations for carrier concentrations 0.75 - 0.9 have precluded SC even here<sup>46</sup>.

### B. Closed-shell ions and negative charge-transfer gap

The traditional approach to arriving at phenomenological minimal Hamiltonians for complex oxides *assumes* that the nominal and true charges (ionicities) of the active cation and the O-ions are the same. The known example of BaBiO<sub>3</sub> (see above) already indicates that this can be incorrect. Physical understanding of this is best obtained within strongly correlated ionic models. What follows merely requires small electron or hole hoppings between the central cation (Bi in BaBiO<sub>3</sub>) and the O-anion, relative to the largest many-electron interactions. For any cation M that can exist in two different valence states M<sup>n+</sup> and M<sup>(n-1)+</sup>, the true ionic charge of the oxide is determined by the inequality<sup>9</sup>

$$I_n + A_2 + \Delta E_{M,n} + \Delta(W) \geq 0 \quad (1)$$

where  $I_n$  is energy of the  $n$ th ionization ( $M^{(n-1)} \rightarrow M^{n+} + e$ ) and  $A_2$  is the second electron-affinity of O. Here  $\Delta E_{M,n} = E_{M,n} - E_{M,n-1}$ , where  $E_{M,n}$  is the Madelung energy of the solid with the cation charge of  $+n$ .  $\Delta(W) = W_n - W_{n-1}$ , where  $W_n$  and  $W_{n-1}$  are the gain in total one-electron delocalization (band) energies of states with cationic charges  $+n$  and  $+(n-1)$ , respectively.  $I_n$  and  $A_2$  are positive, while  $\Delta E_{M,n}$  is negative. Note that, (i)  $W_n$  and  $W_{n-1}$  are both negative, (ii) for cation charge of  $+n$  there are very few charge carriers, while for cation charge  $+(n-1)$  a large fraction of the O-ions (nearly half) are O<sup>1-</sup> and the number of charge carriers is far larger, making  $\Delta(W)$  positive.

The two largest quantities in Eq. 1,  $I_n$  and  $\Delta E_{M,n}$ , have opposite signs and magnitudes several tens of eV or even larger (see below), and are many times larger than  $A_2$  and  $\Delta(W)$ , which are both a few eV. This introduces the possibility of distinct quantum states with nearly integer valences, as opposed to mixed valence<sup>9,47</sup>. For a smaller left hand side in Eq. 1 the ground state occurs as predominantly M<sup>n+</sup>; for a larger left hand side M<sup>(n-1)+</sup> dominates the ground state. Since  $\Delta E_{M,n}$  is nearly independent of the detailed nature of M within a given row of the periodic table, it follows that for *unusually large*  $I_n$  oxides will have strong tendency to be in the ionic state M<sup>(n-1)+</sup>. This conclusion immediately explains the occurrence of only Bi<sup>3+</sup> in BaBiO<sub>3</sub>. As shown in Fig. 1, Bi<sup>3+</sup> with closed shell configuration ([Xe]4f<sup>14</sup>5d<sup>10</sup>6s<sup>2</sup>) has unusually large ionization energy among the three consecutive  $p$ -block elements Pb, Bi and Po in the periodic table.

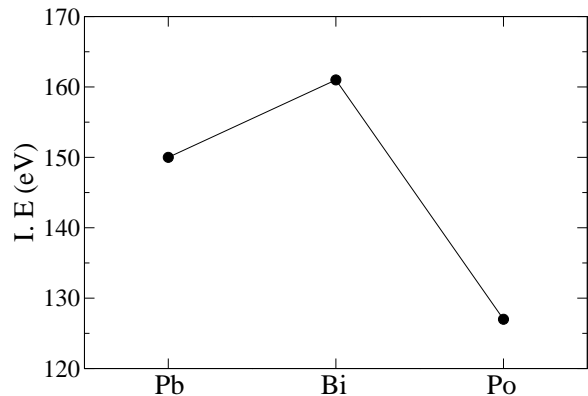


FIG. 1: Fourth ionization energies of Pb, Bi and Po. The absence of Bi<sup>5+</sup> in BaBiO<sub>3</sub> is due to the exceptional stability of Bi<sup>3+</sup>. The plot of second ionization energies of 3d transition metals shows a similar peak at Cu because of the closed-shell nature of Cu<sup>1+</sup>, see Fig. 1 in reference 9.

As with Bi<sup>3+</sup>, unusually large  $n$ th ionization energy is a characteristic of all closed-shell M<sup>(n-1)+</sup>. Additionally, for systems already close to the boundary of the inequality 1, external variables such as temperature, pressure or doping can change  $\Delta E_{M,n}$  or  $\Delta(W)$  enough to lead to first order transition from open-shell M<sup>n+</sup> to closed-shell M<sup>(n-1)+</sup>. The most well-known among such valence transitions are the temperature, pressure and light-induced neutral-to-ionic transitions in the family of mixed-stack organic charge-transfer solids, which have been known for more than four decades<sup>47</sup>. Reference 9 postulated that exactly such a dopant-induced Cu<sup>2+</sup>  $\rightarrow$  Cu<sup>1+</sup> valence transition occurs at the pseudogap transition in the hole-doped cuprates, and at the antiferromagnet-to-superconductor transition in the electron-doped cuprates. The driving forces behind the transition are the unusually high second ionization energy of closed-shell Cu<sup>1+</sup> with closed-shell electron configuration 3d<sup>10</sup> (see Fig. 1 in reference 9), as well as contribution from  $\Delta(W)$  in the doped state, which favors the lower ionicity, because of the far greater number of charge carriers in this state.

The charge-transfer gap following the valence transition is the excitation Cu<sup>1+</sup>O<sup>1-</sup>  $\rightarrow$  Cu<sup>2+</sup>O<sup>2-</sup>, opposite to the excitation in the undoped semiconducting state, and is therefore “negative”. Following valence transition doped cuprates consist of an effective nearly  $\frac{1}{4}$ -filled O hole-band ( $\frac{3}{4}$ -filled electron band) with the closed-shell Cu<sup>1+</sup> playing no significant role<sup>9</sup>. The O-lattice is frustrated, and as has been found from numerically accurate exact diagonalization, quantum Monte Carlo and Path Integral Renormalization Group calculations, a density wave of Cooper pairs as well as a superconducting state occur naturally and uniquely within the frustrated  $\frac{1}{4}$ -filled (and  $\frac{3}{4}$ -filled) band Hubbard Hamiltonian<sup>46,48,49</sup>. This effective *anion-centric one-band model* can describe both hole- and electron-doped cuprates, and aside from explaining correlated-electron SC, is able to give detailed

physical understandings of the spatial broken symmetries in the hole-doped cuprates, the unusual stability of the antiferromagnetic phase in the standard  $T'$  compounds as well as the appearance of SC in undoped thin film  $T'$  cuprates<sup>9</sup>.

Closed-shell characters of  $\text{Cu}^{1+}$  and  $\text{Bi}^{3+}$  are true independent of crystal structure. In octahedral complexes with large CFSE unusually large 4th ionization energy will be true for cations with electron occupancy of  $t_{2g}^5$ . This tendency would be strongest with  $5d$  cations with CFSE much larger than for  $3d$  and  $4d$  cations. Reference 9 therefore proposed that the transition to the pseudogap state in electron-doped  $\text{Sr}_2\text{IrO}_4$  is a consequence the valence transition from  $\text{Ir}^{4+}$  with open-shell configuration  $t_{2g}^5$  to  $\text{Ir}^{3+}$  with closed-shell  $t_{2g}^6$ . As in the cuprates this would again imply a nearly  $\frac{1}{4}$ -filled oxygen hole-band, which would have the tendency to the same charge-ordering and hence the same  $d$ -wave like gap. Strong support for this viewpoint comes from the *known* true charge distribution in octahedral  $\text{IrTe}_2$ . Even as the nominal charges are  $\text{Ir}^{4+}(\text{Te}^{2-})_2$ , the true ionic charges are accepted<sup>50,51</sup> to be  $\text{Ir}^{3+}(\text{Te}^{1.5-})_2$ . Although somewhat unrelated, the occurrence of bulk amounts of  $\text{O}^{1-}-\text{O}^{1-}$  dimers is also not unprecedented and are known to occur below charge-ordering transitions in alkali metal sesquioxides<sup>52-54</sup>  $\text{X}_4\text{O}_6$ ,  $\text{X} = \text{Rb}, \text{Cs}$ .

#### IV. TYPE II NEGATIVE CHARGE-TRANSFER GAP: CATIONS WITH HALF-FILLED SHELLS.

As seen in the previous section, negative charge-transfer is very likely with closed-shell cations and can be driven by both  $\Delta E_{m,n}$  or  $\Delta(W)$ , thereby opening up a new mechanism for IMT. In the following we discuss how a similar IMT can occur in complexes with formal charges close to half-filling.

##### A. The unusually large ionization energies of half-filled ions.

Beyond completely closed-shell cations, isolated free ions that are exactly half-filled also have unusually large ionization energies. For the  $d$ -block elements this is true for ions with electron configurations  $d^5$ , which occur in their high-spin configurations in the free ions because of Hund's coupling. Fig. 2(a) shows that the second ionization energy of Cr ( $\text{Cr}^{1+} \rightarrow \text{Cr}^{2+} + e$ ), the third ionization energy of Mn ( $\text{Mn}^{2+} \rightarrow \text{Mn}^{3+} + e$ ), and the 4th ionization energy of Fe ( $\text{Fe}^{3+} \rightarrow \text{Fe}^{4+} + e$ ) are all significantly larger than those for similarly charged cations neighboring in the periodic table. The behavior seen in Fig. 2(a) for free elements remains true for octahedral complexes of  $3d$  elements where CFSE is weak to moderate and Hund's coupling dominates. Thus octahedral complexes of  $\text{Mn}^{2+}$  are almost universally high-spin, while complexes of  $\text{Fe}^{3+}$  are often high-spin. This co-operative behavior emerges

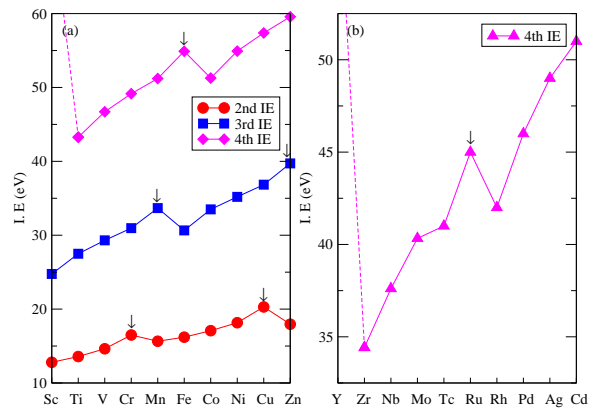


FIG. 2: (a) 2nd, 3rd and 4th ionization energies of  $3d$  transition metals. Note the local maxima on half-filled ions in each case. (b) 4th ionization energies of  $4d$  transition metals. The scales along the y-axes are different in (a) and (b), but the difference in the ionization energies of  $\text{Ru}^{3+}$  and its immediate neighbors in the periodic table is larger than that between  $\text{Cu}^{1+}$  and  $\text{Zn}^{1+}$ .

from the close coupling between high ionization energy and Hund's coupling in the  $3d$  series. This behavior is different with the  $5d$  ions where the much larger CFSE dominates over Hund's coupling, and the closed shell nature of low-spin  $\text{Ir}^{3+}$  drives the  $\text{Ir}^{4+} \rightarrow \text{Ir}^{3+}$  transition. It follows that for  $4d$  cations behavior intermediate between  $3d$  cations with small CFSE and  $5d$  cations with large CFSE can emerge.

##### B. Valence transition and negative charge transfer gap in $\text{Sr}_2\text{RuO}_4$

The nominal charge of the Ru-ion in  $\text{Sr}_2\text{RuO}_4$  and  $\text{Ca}_2\text{RuO}_4$  is  $\text{Ru}^{4+}$  with four  $d$ -electrons. The ion is assumed to be in the low spin state in all prior theoretical work (two experimental studies have however claimed high-spin  $\text{Ru}^{4+}$  in  $\text{Sr}_2\text{RuO}_4$ <sup>55</sup> and metallic  $\text{SrRuO}_3$ <sup>56</sup>). Fig. 2(b) plots the fourth ionization energies of the  $4d$  free elements. As expected, the ionization energy of the isolated  $\text{Ru}^{3+}$  ion is exceptionally large compared to those of  $\text{Tc}^{3+}$  and  $\text{Rh}^{3+}$ , with the differences (4.0 eV and  $\sim 3$  eV, respectively) larger than the difference in the ionization energies of  $\text{Cu}^{1+}$  and  $\text{Zn}^{1+}$  ( $\sim 2$  eV). Should the true charge on the Ru-ions in  $\text{Sr}_2\text{RuO}_4$  be +3 instead of the nominal +4, it would imply that  $\text{Sr}_2\text{RuO}_4$  lies in the same class of materials as bismuthate, cuprate and  $\text{Sr}_2\text{IrO}_4$ .

It is now pointed out that the “rule of thumb” that  $4d$  cations with CFSE larger than  $3d$  cations will be in the low-spin state applies *only when the systems are semiconducting in both the high and low-spin configurations*. Within any low-spin multiband Hubbard model for  $\text{Sr}_2\text{RuO}_4$  and  $\text{Ca}_2\text{RuO}_4$ , depending on the magnitudes of the Hubbard interactions  $U_{xz}$  and  $U_{yz}$  relative to the one-electron hoppings, the system should exhibit

either Mott-Hubbard semiconducting behavior, as is observed in  $\text{Ca}_2\text{RuO}_4$ , or metallic behavior, as observed in  $\text{Sr}_2\text{RuO}_4$ , *but not both*. The difference already suggests that the origin of the metallic behavior of  $\text{Sr}_2\text{RuO}_4$ , along with proximity to ferromagnetism, is not the usual Mott-Hubbard transition. As already pointed out in the previous subsection, understanding the current-induced IMT in  $\text{Ca}_2\text{RuO}_4$ , as well as the diamagnetism in the resultant semimetallic state is also difficult within the simple Mott transition picture. A different theory of the IMT in view of the high ionization energy of high-spin  $\text{Sr}^{3+}$  (see Fig. 2(b)) is presented below. As in the cuprates and bismuthates I compare the relative energies of the  $\text{Sr}_2\text{RuO}_4$  crystal with Sr-ions as *high-spin*  $\text{Ru}^{3+}$  (hereafter labeled as  $|III\rangle$ ) versus low-spin  $\text{Ru}^{4+}$  (labeled as  $|IV\rangle$ ).

Beyond the terms already included in Eq. 1, interactions that determine the relative energies of  $|III\rangle$  and  $|IV\rangle$  include:  $U(\text{CFSE} : j)$ ,  $U(\text{Coulomb}; j)$  and  $U(\text{exchange} : j)$ ,  $|j\rangle = |III\rangle$  and  $|IV\rangle$ , where  $U(\text{CFSE} : j)$  is the crystal field stabilization energy;  $U(\text{Coulomb}; j)$  the direct Coulomb repulsions between electrons occupying the  $d$ -orbitals (Hubbard repulsions between electrons occupying the same as well as different  $d$ -orbitals); and  $U(\text{exchange} : j)$  is the Hund's exchange energy. The inequality that determines the true ionic charge now is,

$$I_n + A_2 + \Delta E_{M,n} + \Delta(W) + \Delta_{CF} + \Delta_C + \Delta_J \geq 0 \quad (2)$$

In the above  $n = 4$  for the case of high-spin  $\text{Ru}^{3+}$  versus low-spin  $\text{Ru}^{4+}$ , and  $A_2$ ,  $\Delta E_{M,n}$  and  $\Delta(W)$  have the same meanings as in Eq. 1.  $\Delta_{CF} = U(\text{CFSE} : III) - U(\text{CFSE} : IV)$  is negative ( $U(\text{CFSE} : III) \simeq 0$ ) and favors state  $|IV\rangle$  over state  $|III\rangle$ , while  $\Delta_J = U(\text{exchange} : III) - U(\text{exchange} : IV)$  is positive and favors state  $|III\rangle$  over state  $|IV\rangle$ . It is difficult to estimate  $\Delta_C = U(\text{Coulomb}; III) - U(\text{Coulomb}; IV)$ ; it is assumed to be small relative to the larger  $\Delta_{CF}$  and  $\Delta_J$ , the competition between which determine the relative stabilities of high versus low-spin in semiconductors. As with Eq. 1, a smaller (larger) left hand side favors larger (smaller) ionicity of Ru.

The following are now pointed out:

(i) First-principles calculations for the cuprates have consistently determined large direct O-O hoppings  $t_{pp} \geq 0.5t_{dp}$  in the cuprates<sup>57,58</sup>, where  $t_{dp}$  involves the  $d_{x^2-y^2}$  orbitals. The  $t_{dp}$  in state  $|IV\rangle$ , however, involves only the  $d_{xy}$  orbitals which is therefore considerably smaller than  $t_{dp}$  in the cuprates. On the other hand, it is reasonable to assume that the magnitudes of  $t_{pp}$  are similar in the two classes of materials. These alone suggest larger  $\Delta(W)$  contribution to the stabilization of  $|III\rangle$  with far larger number of charge carriers over  $|IV\rangle$ .

(ii) The actual contribution by  $\Delta(W)$  to the stabilization of  $|III\rangle$  is even larger, given that in  $|III\rangle$   $t_{dp}$  includes contributions from the  $d_{x^2-y^2}$  orbitals, over and above from  $d_{xy}$ .

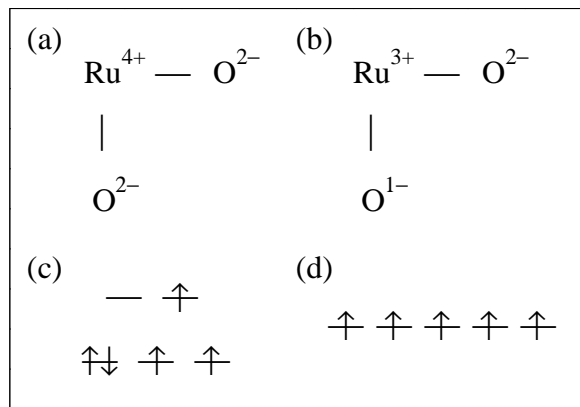


FIG. 3: Schematics of the layer intra-unit cell charge distributions in (a) insulating  $\text{CaRu}_2\text{O}_4$  and (b) metallic  $\text{SrRu}_2\text{O}_4$ . (c) Schematic of the virtual intermediate state in a current-induced ruthenate conductor with an electron added to the low-spin  $\text{Ru}^{4+}$  cation. For strong intra-orbital Coulomb repulsion the extra electron occupies an  $e_g$  orbital and reduces the CFSE self-consistently, which in turn leads to (d) stable  $\text{Ru}^{3+}$  ion in the metallic state with high ionization energy. Charge carriers in the metallic state are entirely on the O-ions in this case.  $\text{Ru}^{3+}$  ions contribute to magnetism but not transport.

(iii)  $\Delta_{CF}$  in Eq. 2 need not be a rigid quantity as in the competition between two semiconductors, where  $\Delta(W) = 0$  by default. When the competition is between a semiconductor and a metal it is likely that  $\Delta_{CF}$  decreases self-consistently with conduction, since a wide O-ion bandwidth requires  $e_g$  occupancy and hence smaller  $\Delta_{CF}$  (see Fig. 3).

Based on the above I posit that valence transition from low-spin  $\text{Ru}^{4+}$  to high-spin  $\text{Ru}^{3+}$  is the origin of the metallic behavior of  $\text{Sr}_2\text{RuO}_4$ . As a consequence of the valence transition there is a preponderance of layer  $\text{O}^{1-}$  ions instead of a few due to self-doping. In Fig. 3(a) and (b) schematics of the IMT in oxides with large ionization energies of  $\text{M}^{(n-1)+}$  are shown, while the schematics in Fig. 3(c) and (d) refer to the current-induced  $\text{Ru}^{4+} \rightarrow \text{Ru}^{3+}$  transition. The difference between  $\text{Ca}_2\text{RuO}_4$  and  $\text{Sr}_2\text{RuO}_4$  is ascribed to the much smaller size of the Cation leading to larger  $\Delta E_{M,n}$  for  $\text{Ca}_2\text{RuO}_4$  in Eq. 2, that favors  $\text{Ru}^{4+}$ . It is shown in the next section that straightforward explanations of the experimental results presented in section II that are difficult to understand with low-spin  $\text{Ru}^{4+}$  are obtained within the negative charge-transfer gap model in which Ru-ions occur as high-spin  $\text{Ru}^{3+}$  which contribute to magnetism but not transport.

## V. EXPERIMENTAL RAMIFICATIONS OF THE VALENCE TRANSITION MODEL.

### A. $\text{Sr}_2\text{RuO}_4$

(i) *d-wave SC*. Within the valence transition model the charge-carriers are entirely on the O-ions which have average charge  $-1.5$ . The  $\text{Ru}^{3+}$ -ions play at most a virtual role in transport, exactly as the closed-shell  $\text{Cu}^{1+}$  ions in the cuprates<sup>9</sup>. Fig. 4 shows the charge-carrying checkerboard O-sublattice of the  $\text{RuO}_2$  layer, rotated  $45^\circ$  relative to the Ru-O-Ru bonds. The effective Hamiltonian  $H_{eff}$  for the charge carriers on the checkerboard lattice is,

$$H_{eff} = - \sum_{\langle ij \rangle, \sigma} t_{pp} (p_{i,\sigma}^\dagger p_{j,\sigma} + H.c.) \quad (3)$$

$$- \sum_{[ij], \sigma} t_{pdp} (p_{i,\sigma}^\dagger p_{j,\sigma} + H.c.) + U_p \sum_i n_{p_i, \uparrow} n_{p_i, \downarrow}$$

$$\frac{1}{2} \sum_{\langle ij \rangle} V_p^{NN} n_{p_i} n_{p_j} + \frac{1}{2} \sum_{(ij)} V_p^{NNN} n_{p_i} n_{p_j}$$

Here  $p_{i,\sigma}^\dagger$  creates a hole ( $\text{O}^{1-}$ ) on the  $p$ -orbital of an  $\text{O}^{2-}$  ion,  $n_{p_i, \sigma} = p_{i,\sigma}^\dagger p_{i,\sigma}$  and  $n_p = \sum_{\sigma=\uparrow, \downarrow} n_{p_i, \sigma}$ . Sums are over the O-ions in the  $\text{RuO}_2$  layer,  $\langle \rangle$  denotes nearest neighbor (nn) oxygens;  $[ \ ]$  denotes O-ions linked via the same  $\text{Ru}^{3+}$ -ion (nn and nnn O-ions are linked by Ru-O bonds at  $90^\circ$  and  $180^\circ$  degrees, respectively); and  $( \ )$  are nnn O-ions irrespective of whether they are linked via the same Ru-ion or not.  $U_p$ ,  $V_p^{NN}$  and  $V_p^{NNN}$  are Coulomb repulsions between pairs of holes on the same, nn and nnn  $p$ -orbitals, respectively. The hopping parameter  $t_{pp}$  is the direct hopping between nn O-ions while  $t_{pdp}$  is the effective hopping between nn and nnn O-ions linked by the same  $\text{Ru}^{3+}$  ion,  $t_{pdp} = t_{dp}^2 / \Delta E$ ,  $t_{dp}$  is the hopping between a Ru  $d$ -orbital and oxygen  $p$ -orbital and  $\Delta E = E(\text{Ru}^{3+}\text{O}^{1-}) - E(\text{Ru}^{4+}\text{O}^{2-})$ . The large ionization energy of  $\text{Ru}^{3+}$  implies large  $\Delta E$ , which is likely to make  $t_{pdp} < t_{pp}$ .

Given the  $S = 5/2$  spin state of  $\text{Ru}^{3+}$ , for  $t_{pp} = 0$  ferromagnetic spin coupling between  $\text{O}^{1-} - \text{O}^{1-}$  would have been expected. For  $t_{pp} > t_{pdp}$  anticipated here, spin singlet coupling dominates. Sophisticated quantum mechanical calculations by the present author and colleagues<sup>46,48,49</sup> using exact diagonalization, Constrained Path Quantum Monte Carlo and Path Integral Renormalization Group calculations have consistently shown that singlet superconducting pair-pair correlations are uniquely enhanced by the Hubbard interaction (relative to the noninteracting model) at  $\frac{3}{4}$ -filling and a narrow carrier density region about it on a geometrically frustrated lattice. At all other fillings the Hubbard interaction suppresses the pair-pair correlations relative to the noninteracting ( $U_p = V_p^{NN} = V_p^{NNN} = 0$ ) Hamiltonian, a result that agrees with the conclusions of reference 45. Very recently, Clay and Roy have further shown that again uniquely at this same filling, Su-Schrieffer-Heeger

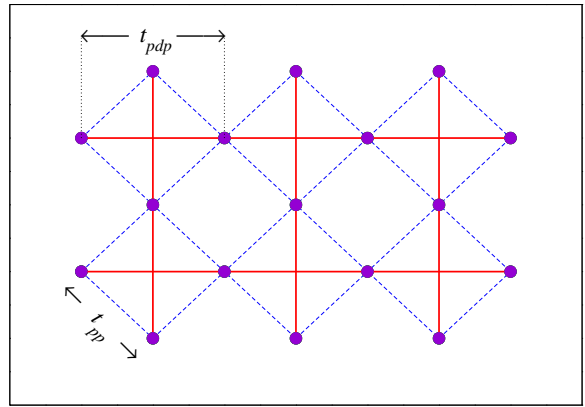


FIG. 4: The checkerboard lattice of O-ions, common to both  $\text{Sr}_2\text{RuO}_4$  and cuprates, in their superconducting states. The half-filled  $\text{Ru}^{3+}$  (closed-shell  $\text{Cu}^{1+}$ ) cations, which occur at the intersections of the solid lines, are not explicitly shown as they do not play any role in superconductivity, which involves only the  $\frac{3}{4}$ -filled O-band. The nearest neighbor direct O-O hoppings  $t_{pp}$ , as well as the O-O hoppings via the metal cations,  $t_{pdp}$  (see text), are shown. The magnitudes of  $t_{pdp}$  are the same for O-M-O bond angles of  $90^\circ$  and  $180^\circ$ , and are much larger for cuprates than for  $\text{Sr}_2\text{RuO}_4$ . In the latter it is anticipated that  $t_{pp} > t_{pdp}$  (see text).

bond phonons and the Hubbard  $U$  act co-operatively to further enhance the superconducting pair-pair correlation, while no such co-operative interaction is found at any other filling<sup>59</sup>.

The superconducting state in the frustrated  $\frac{3}{4}$ -filled band evolves from a commensurate CDW of Cooper pairs, - a paired-electron crystal (PEC) - that is unique to the exactly  $\frac{3}{4}$ -filled frustrated lattice<sup>60,61</sup>. Beyond cuprates, this theory of correlated-electron SC readily explains the limitation of SC<sup>39,41</sup> to relatively narrow carrier concentration range  $0.37 \leq x \leq 0.5$  in  $\text{Ba}_{1-x}\text{K}_x\text{BiO}_3$ , for which, as of now there exists no other clear explanation. With the Bi-ions occurring only as  $\text{Bi}^{3+}$ , as determined experimentally<sup>39,40</sup> the charge on the O-ions ranges from 1.50-1.54 for this range of  $x$ . The  $s$ -wave symmetry here is a natural consequence of the three-dimensional O-lattice in  $\text{Ba}_{1-x}\text{K}_x\text{BiO}_3$ .

(ii) *Muon-spin rotation and apparent time-reversal breaking*. The apparent broken time reversal symmetry is associated with the ferromagnetic  $\text{Ru}^{3+}$ - $\text{Ru}^{3+}$  spin-spin coupling, which, however, is unrelated to the SC itself. This is also the simplest explanation for the invariance of the Josephson critical current under the inversion of current and magnetic fields<sup>16</sup>: SC involves the O-ions only and not the Ru-ions. It is very likely that the same mechanism of transport applies also to the ferromagnetic metal  $\text{SrRuO}_3$ , which has been thought to be an itinerant ferromagnet, A model-specific prediction is made in the next section.

(iii)  *$T_c$  enhancement by the application of uniaxial pressure*. Carrier density-dependent calculations of superconducting pair-pair correlations have found

that these are enhanced relative to the noninteracting Hamiltonian over a region of small width about  $\frac{3}{4}$ -filling, with the strongest correlations occurring for exactly  $\frac{3}{4}$ -filling<sup>48,49,62</sup>. The implication for this is that should the filling be less than exactly  $\frac{3}{4}$  (as it should be under ambient pressure, since integral charges require complete reverse charge transfer  $\text{Ru}^{4+}(\text{O}^{2-})_2 \rightarrow \text{Ru}^{3+}(\text{O}^{2-})_1(\text{O}^{1-})_1$ )  $T_c$  will be less than the maximum possible. Within the valence transition model, pressure along the Ru-O bonds (but not along the Ru-Ru diagonal direction) enhances the reverse charge-transfer because of the increase in  $t_{dp}$ .

### B. $\text{Ca}_2\text{RuO}_4$ and $\text{Ca}_{2-x}\text{Sr}_x\text{RuO}_4$

(i) *Current-induced IMT and diamagnetism.* There is no explanation of the current-induced IMT<sup>26,27</sup> and diamagnetism<sup>28</sup> within the usual models of Mott transition. Within the valence transition model the IMT is driven by the large  $\Delta(W)$  within Eq. 2, giving a current-carrying state whose structure is very different from the insulator (see Fig. 3), with nearly half the O-ions occurring as  $\text{O}^{1-}$ . As mentioned above, the correlated  $\frac{3}{4}$ -filled geometrically frustrated lattice exhibits a strong tendency to form a commensurate paired-electron crystal (PEC)<sup>60,61</sup>, with nearest neighbor spin-singlets separated by pairs of vacancies (corresponding to periodic  $\text{O}^{1-}-\text{O}^{1-}-\text{O}^{2-}-\text{O}^{2-}$ ). Reference 9 has pointed out that the charge-ordered state in the cuprates (and many other systems with the same carrier density) can be understood within the same picture. The concept of the PEC is identical to the concept of density-wave of Cooper pairs that has been conjectured by many authors to be proximate to the superconducting state in the cuprates<sup>63-66</sup>. With increased frustration, the PEC gives way to a paired-electron liquid and ultimately to a superconductor<sup>48,49,62</sup>. The current-driven semimetallic state in  $\text{Ca}_2\text{RuO}_4$  is a weakly fluctuating PEC, and hence diamagnetic.

The above explanation is also sufficient for understanding the different crystal structures of the current-induced metallic state and  $\text{Ca}_{2-x}\text{Sr}_x\text{RuO}_4$  from that reached by temperature and pressure-induced IMT in  $\text{CaRu}_2\text{O}_4$ . The latter transitions correspond to the usual Mott-Hubbard transition in the low-spin  $\text{Ru}^{4+}$ -based system.

## VI. EXPERIMENTAL PREDICTIONS.

Here I make experimental predictions specific to the negative charge-transfer gap model.

(i) *Charge densities on the layer oxygens.*  $^{17}\text{O}$  NMR experiments should be able to find the charge densities on the layer oxygens. It is predicted that this charge density in  $\text{Sr}_2\text{RuO}_4$  in the superconducting state is  $-1.5$ .

(ii) *Spin susceptibility due to Ru-ions.* As of writing Knight-shift measurements have been repeated only for the O-sites<sup>7,8</sup>. The earlier literature also reported extensive measurements of Ru-ion spin susceptibility through  $T_c$ .  $^{99}\text{Ru}$  Knight-shift measurement with the magnetic field parallel to the  $\text{RuO}_2$  layer<sup>67</sup>, and  $^{101}\text{Ru}$  Knight-shift measurements with the field perpendicular to the layer<sup>68</sup> both showed that the spin susceptibility due to Ru-ions remained unchanged below  $T_c$ . *It is predicted that these observations will remain unaltered.* If found to be true this will be the strongest proof that the Ru-ions do not participate in normal state transport and SC in  $\text{Sr}_2\text{RuO}_4$ . (iii) It is conceivable that in the current-induced diamagnetic state of  $\text{CaRu}_2\text{O}_4$  O-ions with two different oxygen charge densities can be detected by  $^{17}\text{O}$  NMR. This is a condition for the formation of an O-based fluctuating PEC. Actual observation of the fluctuating CDW may be difficult, in part because the populations of the layer O-ions with smaller and larger charge densities are the same. Previous  $^{17}\text{O}$ -NMR, however, successfully determined the intra-unit cell inequivalency among the O-ions in  $\text{YBa}_2\text{Cu}_3\text{O}_y$ <sup>30,33</sup>.

## VII. CONCLUSIONS

In conclusion, nominal and true charges in conducting perovskite oxides can be very different. In particular, it is not necessarily true that the natural state of oxide ions is  $\text{O}^{2-}$ . The second electron affinity of O is positive (it costs energy to add the second extra electron) and it is only the gain in Madelung energy in the insulating oxides that drives a metal oxide to a state with high cation charge  $M^{n+}$  and anion charge  $\text{O}^{2-}$ . For systems in which cations can have lower charge  $M^{(n-1)+}$  with high ionization energy, IMT occurs via a valence transition  $M^{n+} \rightarrow M^{(n-1)+}$ , which in the quasi-2D materials leaves the layers with  $\frac{3}{4}$ -filled band of electrons. In undoped  $\text{BaBiO}_3$  with skipped valency the competition is between  $\text{Bi}^{3+}$  and  $\text{Bi}^{5+}$ , and the very high ionization energy of closed-shell  $\text{Bi}^{3+}$  precludes even higher ionic charge. Replacement of Ba with K leads to SC, but only with K concentration that once again gives a nearly  $\frac{3}{4}$ -filled band of electrons. The  $s$ -wave SC here is due to the 3D nature of the O-sublattice and does not contradict any of the other conclusions.

The above theory gives the simplest and most comprehensive explanations for the apparently peculiar observations in  $\text{Sr}_2\text{RuO}_4$ . The  $\text{Ru}^{3+}$  ions are responsible for the magnetic behavior but the charge carriers are entirely on the O-sites. The superconducting pairing involves  $\text{O}^{1-}-\text{O}^{1-}$  dimers and is  $d$ -wave spin singlet. The theory explains simultaneously the drop in spin susceptibility due to O-ions<sup>7,8</sup>, the earlier muon-spin rotation measurements that suggested broken time-reversal symmetry<sup>14</sup>, and also the latest experiments that have found time-reversal invariant SC<sup>16</sup>. Ru-ions have higher charge  $\text{Ru}^{4+}$  and low spin in  $\text{Ca}_2\text{RuO}_4$  because of the smaller size of



$\text{Ca}^{2+}$  relative to  $\text{Sr}^{2+}$ , that contributes to larger gain in Madelung energy stabilization. The system nevertheless is close to the inequality in Eq. 2, and the large gain in  $\Delta(W)$  drives the current-induced IMT. The diamagnetism in the semimetallic state with even smaller current is *expected* within the fluctuating PEC in the correlated  $\frac{3}{4}$ -filled band<sup>60,61</sup>.

The uniqueness of the  $\frac{3}{4}$  or  $\frac{1}{4}$ -filled frustrated lattice, in the context of correlated-electron SC, has been discussed before extensively by the present author and collaborators. It is only here that a commensurate CDW of nearest neighbor spin-dimers can occur<sup>60,61</sup>, and the dimers can be mobile for frustration exceeding a threshold<sup>46,48,49</sup>. The bound dimers move through the paired vacant sites, and the gain in delocalization energy is largest at a filling where the number of occupied dimer sites and number of

paired vacancies are equal. This confers the greatest stabilization against pair breaking.

## VIII. ACKNOWLEDGMENTS

The author acknowledges support from NSF grant CHE-1764152 and is grateful to Drs. R. Torsten Clay (Mississippi State University), Charles Stafford (University of Arizona) and Shufeng Zhang (University of Arizona) for their careful readings of the manuscript and suggestions. The author also acknowledges close interactions and collaborations through the years with Dr. Clay.

- 
- <sup>1</sup> A. P. Mackenzie and Y. Maeno, *Rev. Mod. Phys.* **75**, 657 (2003).
  - <sup>2</sup> A. P. Mackenzie, T. Scaffidi, C. W. Hicks, and Y. Maeno, *npj Quantum Materials* (2017).
  - <sup>3</sup> C. W. Hicks, D. O. Brodsky, E. A. Yelland, A. S. Gibbs, J. A. N. Bruin, M. E. Barber, S. D. Edkins, K. Nishimura, S. Yonezawa, Y. Maeno, et al., *Science* **344**, 283 (2014).
  - <sup>4</sup> H. Taniguchi, K. Nishimura, S. K. Goh, S. Yonezawa, and Y. Maeno, *J. Phys. Soc. Jpn.* **84**, 014707 (2015).
  - <sup>5</sup> A. Steppke, L. Zhao, M. E. Barber, T. Scaffidi, F. Jerzembeck, H. Rosner, A. S. Gibbs, Y. Maeno, S. H. Simon, A. P. Mackenzie, et al., *Science* **355**, eaaf9398 (2017).
  - <sup>6</sup> E. Hassinger, P. Bourgeois-Hope, H. Taniguchi, S. R. de Cotret, G. Grissonnanche, M. S. Anwar, Y. Maeno, N. Doiron-Leyraud, and L. Taillefer, *Phys. Rev. X* **7**, 011032 (2017).
  - <sup>7</sup> Y. Luo et al., *Phys. Rev. X* **9**, 021044 (2019).
  - <sup>8</sup> A. Pustogow, Y. Luo, A. Chronister, Y.-S. Su, D. A. Sokolov, F. Jerzembeck, A. P. Mackenzie, C. W. Hicks, N. Kikugawa, S. Raghu, et al., *Nature* **574**, 72 (2019).
  - <sup>9</sup> S. Mazumdar, *Phys. Rev. B* **98**, 205153 (2018).
  - <sup>10</sup> A. de la Torre, S. M. Walker, F. Bruno, S. Ricco, Z. Wang, I. G. Lezama, G. Scheerer, G. Girit, D. Jaccard, C. Berthod, et al., *Phys. Rev. Lett.* **115**, 176402 (2015).
  - <sup>11</sup> Y. H. Kim, N. H. Sung, J. D. Denlinger, and B. J. Kim, *Nat. Phys.* **12**, 37 (2016).
  - <sup>12</sup> I. Battisti, K. M. Bastiaans, V. Fedoseev, A. de la Torre, N. Iliopoulos, A. Tamai, E. C. Hunter, R. S. Perry, J. Zaanen, F. Baumberger, et al., *Nat. Phys.* **13**, 21 (2017).
  - <sup>13</sup> K. Ishida, H. Mukuda, Y. Kitaoka, K. Asayama, Z. Q. Mao, Y. Mori, and Y. Maeno, *Nature* **396**, 658 (1998).
  - <sup>14</sup> G. M. Luke, Y. Fudamoto, K. M. Kojima, M. I. Larkin, J. Merrin, B. Nachumi, Y. J. Uemura, Y. Maeno, Z. Q. Mao, Y. Mori, et al., *Nature* **394**, 558 (1998).
  - <sup>15</sup> J. Xia, Y. Maeno, P. T. Beyersdorf, M. M. Fejer, and A. Kapitulnik, *Phys. Rev. Lett.* **97**, 167002 (2006).
  - <sup>16</sup> S. Kashiwaya, K. Saitoh, H. K. M. Koyanagi, M. Sato, K. Yada, and Y. T. Y. Maeno, *Phys. Rev. B* **100**, 094530 (2019).
  - <sup>17</sup> H. Karapetyan, M. Hucker, G. D. Gu, J. M. Tranquada, M. M. Fejer, J. Xia, and A. Kapitulnik, *Phys. Rev. Lett.* **109**, 147001 (2012).
  - <sup>18</sup> S. Yonezawa, T. Kajikawa, and Y. Maeno, *Phys. Rev. Lett.* **110**, 077003 (2013).
  - <sup>19</sup> M. Braden, G. Andre, S. Nakatsuji, and Y. Maeno, *Phys. Rev. B* **58**, 847 (1998).
  - <sup>20</sup> O. Friedt, M. Braden, G. Andre, P. Adelman, S. Nakatsuji, and Y. Maeno, *Phys. Rev. B* **63**, 174432 (2001).
  - <sup>21</sup> H. Fukazawa and Y. Maeno, *J. Phys. Soc. Jpn.* **70**, 460 (2001).
  - <sup>22</sup> S. Nakatsuji, V. Dobrosavljevic, D. Tanaskovic, M. Minakata, H. Fukazawa, and Y. Maeno, *Phys. Rev. Lett.* **93**, 146401 (2004).
  - <sup>23</sup> A. Liebsch and H. Ishida, *Phys. Rev. Lett.* **98**, 216403 (2007).
  - <sup>24</sup> E. Gorelov, M. Karolak, T. O. Wehling, F. Lechermann, A. I. Lichtenstein, and E. Pavarini, *Phys. Rev. Lett.* **104**, 226401 (2010).
  - <sup>25</sup> F. Nakamura, T. Goko, M. Ito, T. Fujita, S. Nakatsuji, H. Fukazawa, Y. Maeno, P. Alireza, D. Forsythe, and S. R. Julian, *Phys. Rev. B* **65**, 220402(R) (2002).
  - <sup>26</sup> F. Nakamura, M. Sakaki, Y. Yamanaka, S. Tamaru, T. Suzuki, and Y. Maeno, *Sci. Rep.* **3**, 2536 (2013).
  - <sup>27</sup> R. Okazaki, Y. Nishina, Y. Yasui, F. Nakamura, T. Suzuki, and I. Terasaki, *J. Phys. Soc. Jpn.* **82**, 103702 (2013).
  - <sup>28</sup> C. Sow, S. Yonezawa, S. Kitamura, T. Oka, K. Kuroki, F. Nakamura, and Y. Maeno, *Science* **358**, 1084 (2017).
  - <sup>29</sup> J. Bertinshaw et al., *Phys. Rev. Lett.* **123**, 137204 (2019).
  - <sup>30</sup> T. Wu, H. Mayaffre, S. Kraemer, M. Horvatic, C. Berthier, W. N. Hardy, L. Ruixing, D. A. Bonn, and M.-H. Julien, *Nat. Commun.* **6**, 6438 (2015).
  - <sup>31</sup> Y. Kohsaka, T. Hanaguri, M. Azuma, M. Takano, J. C. Davis, and H. Takagi, *Nat. Phys.* **8**, 534 (2012).
  - <sup>32</sup> R. Comin, R. Sutarto, F. He, E. H. D. S. Neto, L. Chauviere, A. Frano, R. Liang, W. N. Hardy, D. A. Bonn, Y. Yoshida, et al., *Nature Materials* **14**, 796 (2015).
  - <sup>33</sup> S. Reichardt, M. Jurkutat, R. Guehne, J. Kohlrautz, A. Erb, and J. Haase, *Condensed Matter* **3**, 23 (2018).
  - <sup>34</sup> N. P. Armitage, P. Fournier, and R. L. Greene, *Rev. Mod. Phys.* **82**, 2421 (2010).
  - <sup>35</sup> M. Naito, Y. Krockenberger, A. Ikeda, and H. Yamamoto, *Physica C* **523**, 28 (2016).
  - <sup>36</sup> E. H. D. S. Neto, R. Comin, F. He, R. Sutarto, Y. Jiang, R. L. Greene, G. A. Sawatzky, and A. Damascelli, *Science*

- 347**, 282 (2015).
- <sup>37</sup> E. H. D. S. Neto, B. Yu, M. Minola, R. Sutarto, E. Schierle, F. Boschini, M. Zonno, M. Bluschke, J. Higgins, Y. Li, et al., *Sci. Adv.* **2**, e1600782 (2016).
- <sup>38</sup> T. M. Rice and L. Sneddon, *Phys. Rev. Lett.* **47**, 689 (1981).
- <sup>39</sup> N. C. Plumb, D. J. Gawryluk, Y. Wang, Z. Ristic, J. Park, B. Q. Lv, Z. Wang, C. E. Matt, N. Xu, T. Shang, et al., *Phys. Rev. Lett.* **117**, 037002 (2016).
- <sup>40</sup> A. Khazraie, K. Foyevtsova, I. Elfimov, and G. A. Sawatzky, *Phys. Rev. B* **97**, 075103 (2018).
- <sup>41</sup> S. Pei, J. D. Jorgensen, B. Dabrowski, D. G. Hinks, D. R. Richards, and A. W. Mitchell, *Phys. Rev. B* **41**, 4126 (1990).
- <sup>42</sup> B. J. Kim, H. Jin, S. J. Moon, J.-Y. Kim, B.-G. Park, C. S. Leem, J. Yu, T. W. Noh, C. Kim, S.-J. Oh, et al., *Phys. Rev. Lett.* **101**, 076402 (2008).
- <sup>43</sup> Y. J. Yan, M. Ren, H. Xu, B. Xie, R. Tao, H. Choi, N. Lee, Y. Choi, T. Zhang, and D. Feng, *Phys. Rev. X* **5**, 041018 (2015).
- <sup>44</sup> M. Hashimoto, I. M. Vishik, R.-H. He, T. P. Devereaux, and Z.-X. Shen, *Nat. Phys.* **10**, 483 (2014).
- <sup>45</sup> C.-M. C. M. Qin, H. Shi, E. Vitali, C. Hubig, S. R. W. U. Schöllöck, and S. Zhang, arXiv:1910.08931 (2019).
- <sup>46</sup> N. Gomes, W. W. D. Silva, T. Dutta, R. T. Clay, and S. Mazumdar, *Phys. Rev. B* **93**, 165110 (2016).
- <sup>47</sup> M. Masino, N. Castagnetti, and A. Girlando, *Crystals* **7**, 108 (2017).
- <sup>48</sup> W. W. D. Silva, N. Gomes, S. Mazumdar, and R. T. Clay, *Phys. Rev. B* **93**, 205111 (2016).
- <sup>49</sup> R. T. Clay and S. Mazumdar, *Phys. Reports* **788**, 1 (2019).
- <sup>50</sup> Y. S. Oh, J. J. Yang, Y. Horibe, and S.-W. Cheong, *Phys. Rev. Lett.* **110**, 127209 (2013).
- <sup>51</sup> A. F. Fang, G. Xu, T. Dong, P. Zheng, and N. L. Wang, *Sci. Rep.* **3**, 1153 (2013).
- <sup>52</sup> P. Adler et al., *Sci. Adv.* **4**, eaap7581 (2018).
- <sup>53</sup> R. H. Colman, H. E. Okur, W. Kockelmann, C. M. Brown, S. Annette, C. Felser, M. Jansen, and K. Prassides, *Inorg. Chem.* **58**, 14532 (2019).
- <sup>54</sup> T. Knaflic, P. Jeglic, M. Komelj, A. Zorko, P. K. Biswas, A. N. Ponomaryov, S. A. Zvyagin, M. Reehuis, A. Hoser, M. Geiss, et al., *Phys. Rev. B* **101**, 024419 (2020).
- <sup>55</sup> M. Itoh, M. Shikano, and T. Shimura, *Phys. Rev. B* **51**, 16432 (1995).
- <sup>56</sup> A. J. Grutter, F. J. Wong, E. Arenholz, A. Vailionis, and Y. Suzuki, *Phys. Rev. B* **85**, 134429 (2012).
- <sup>57</sup> M. Hirayama, Y. Yamaji, T. Misawa, and M. Imada, *Phys. Rev. B* **98**, 638,2 85134501 (2018).
- <sup>58</sup> M. Hirayama, T. Misawa, T. Ohgoe, Y. Yamaji, and M. Imada, *Phys. Rev. B* **99**, 245155 (2019).
- <sup>59</sup> R. T. Clay and D. Roy, arXiv:1911.06158 (2020).
- <sup>60</sup> H. Li, R. T. Clay, and S. Mazumdar, *J. Phys.: Condens. Matter* **22**, 272201 (2010).
- <sup>61</sup> S. Dayal, R. T. Clay, H. Li, and S. Mazumdar, *Phys. Rev. B* **83**, 245106 (2011).
- <sup>62</sup> N. Gomes, R. T. Clay, and S. Mazumdar, *J. Phys. Condens. Matter* **25**, 385603 (2013).
- <sup>63</sup> M. Franz, *Nature* **305**, 1410 (2004).
- <sup>64</sup> H.-D. Chen, O. Vafek, A. Yazdani, and S.-C. Zhang, *Phys. Rev. Lett.* **93**, 187002 (2004).
- <sup>65</sup> Z. Tesanovic, *Phys. Rev. Lett.* **93**, 217004 (2004).
- <sup>66</sup> M. H. Hamidian, S. D. Edkins, S. H. Joo, A. Kostin, H. Eisaki, S. Uchida, M. J. Lawler, E.-A. Kim, A. P. Mackenzie, K. Fujita, et al., *Nature* **532**, 343 (2016).
- <sup>67</sup> K. Ishida, H. Mukuda, Y. Kitaoka, Z. Q. Mao, H. Fukazawa, and Y. Maeno, *Phys. Rev. B* **63**, 060507(R) (2001).
- <sup>68</sup> K. Ishida, H. Murakawa, H. Mukuda, Y. Kitaoka, Z. Q. Mao, and Y. Maeno, *J. Phys. Chem. Solids* **69**, 3108 (2008).